Drought Monitoring Using the Sentinel-3-Based Multiyear Vegetation Temperature Condition Index in the Guanzhong Plain, China

Xijia Zhou, Pengxin Wang, Kevin Tansey, Darren Ghent, Shuyu Zhang, Hongmei Li, and Lei Wang

***Abstract*—The vegetation temperature condition index (VTCI) has been shown to perform well for drought monitoring using multiyear advanced very high-resolution radiometer (AVHRR) and moderate resolution imaging spectroradiometer (MODIS) data. Compared to single-year VTCI, the VTCI calculated by multiyear data can quantitatively reflect the degree of drought and precipitation in a region. Sentinel-3 is a recently launched remote sensing satellite with high temporal resolution and is similar to the satellites carrying AVHRR and MODIS sensors. One year of Sentinel-3 data is available for calculating the VTCI, and given the need for developing quantitatively drought monitoring capabilities, the aim of this study is to investigate the methods used to calculate the potential multiyear Sentinel-3 VTCI for quantitative drought monitoring. This is based on a comparison with multiyear Terra MODIS VTCI and a correlation analysis with cumulative precipitation data. The analysis results indicate that the potential multiyear Sentinel-3 VTCI can be accurately calculated from the single-year Sentinel-3 VTCI based on the linear correlation between the single-year VTCI and multiyear VTCI derived from Terra MODIS, which do not exhibit obvious systematic deviations from the multiyear Terra MODIS VTCI (the absolute value of the average bias $<$0.04). The multiyear Sentinel-3 VTCIs can quantitatively reflect the drought levels, which are significantly correlated with the recent cumulative precipitation throughout the study period ($R^2 = 0.731$, $P < 0.001$). Therefore, it is proposed that Sentinel-3 can successfully inherit the VTCI-based drought monitoring tasks from MODIS.**

***Index Terms*—Drought monitoring, moderate resolution imaging spectroradiometer (MODIS), Sentinel-3, vegetation temperature condition index (VTCI).**

I. Introduction

DROUGHT is one of the most important factors that influence crop yields. Drought can seriously threaten water and food security and may lead to a reduction in crop yield [1], [2]. Therefore, it is necessary to monitor droughts quickly and accurately. Traditional crop drought monitoring is usually measured in fields and at meteorological stations using data with high temporal resolution such as soil moisture and precipitation. However, these data are point-based, and it is difficult to accurately obtain a continuous spatial distribution of drought conditions [3], [4].

Remote sensing data can capture, in a continuous manner, the spatial distribution of drought, which cannot be captured by ground measurements. The Normalized Difference Vegetation Index (NDVI) has been successfully used for global drought monitoring. NDVI itself has no direct quantitative relationship with drought. It has been reported that the relationship between the current NDVI and multiyear NDVI can reflect the degree of drought. For example, the maximum and minimum NDVI values in multiple years were used to change the current NDVI into the Vegetation Condition Index (VCI) [5], which reflects how close the NDVI in the current period is to the minimum NDVI over multiple years. However, the VCI cannot accurately monitor drought in some cases, such as when soil moisture is excessive [6]. Drought monitoring using the VCI combined with the temperature condition index (TCI) can more accurately reflect the area and intensity of drought. The calculation formula for the TCI is similar to that for the VCI, which replaces NDVI with land surface temperature (LST) and indicates how close the LST in the current period is to the maximum LST over multiple years. The TCI can be used to monitor the temperature-related vegetation stress and the stress caused by excess soil moisture [6]. In addition, researchers found that the two-dimensional scatterplots of NDVI and LST are triangular at the regional scale [7], [8]. Based on this, the vegetation TCI (VTCI) was developed for drought monitoring. The results indicate that the VTCI exhibits good performance in classifying the relatively dry–wet conditions in the Guanzhong Plain [9]. Thereafter, the methods for determining the multiyear warm edge and cold edge

Manuscript received June 28, 2019; revised October 24, 2019; accepted November 13, 2019. Date of publication December 2, 2019; date of current version February 12, 2020. This work was supported in part by the National Natural Science Foundation of China under Grants 41871336 and 41811530303 and in part an Agri-Tech in China Newton Network+ (ATCNN) Small Project Award awarded by Rothamsted Research (UK) on behalf of the Science & Technology Facilities Council (STFC). The work of D. Ghent was supported in part by the National Centre for Earth Observation (NCEO) in the U.K. *(Corresponding author: Pengxin Wang.)*

X. Zhou, P. Wang, and L. Wang are with the College of Information and Electrical Engineering, China Agricultural University and Key Laboratory of Remote Sensing for Agri-Hazards, Ministry of Agriculture and Rural Affairs, Beijing 100083, China (e-mail: zxj1992@cau.edu.cn; wangpx@cau.edu.cn; leiwangciee2015@cau.edu.cn).

K. Tansey is with the School of Geography, Geology and the Environment and Centre for Landscape and Climate Research, University of Leicester, Leicester LE1 7RH, U.K. (e-mail: kjt7@le.ac.uk).

D. Ghent is with the National Centre for Earth Observation (NCEO) Department of Physics and Astronomy, University of Leicester, Leicester LE1 7RH, U.K. (e-mail: djg20@leicester.ac.uk).

S. Zhang and H. Li are with the Shaanxi Provincial Meteorological Bureau, Xi'an 710014, China (e-mail: shuyuzhang88@sina.com; lee8003@163.com).

Digital Object Identifier 10.1109/JSTARS.2019.2953955

for the VTCI were developed [10]. Since the drought levels in a region do not range from extreme drought to extreme humidity in a short period, the VTCI calculated using the single-year warm edge and cold edge (called the single-year VTCI below) can only reflect the relatively dry–wet conditions. However, similar to the TCI, the VTCI calculated using the multiyear warm edge and cold edge (called the multiyear VTCI below) reflects the drought level over multiple years. It is considered that the drought levels in a region can range from extreme drought to extreme humidity in multiple years. Therefore, the multiyear VTCI is a comparable quantitative drought monitoring result over a given 10-day interval in different years. At present, the VTCI has been successfully used for drought monitoring in the Guanzhong Plain of China, the Great Plains of the United States, and Punjab in Pakistan. These results show that the VTCI exhibits strong correlations with both cumulative precipitation and soil moisture [10]–[13].

To date, advanced very high-resolution radiometer (AVHRR) and moderate resolution imaging spectroradiometer (MODIS) images have been successfully used for drought monitoring with the VTCI. MODIS sensors are still available but have been operational for almost 20 years. Drought monitoring systems based on NDVI and LST could be affected should MODIS sensors become unavailable. Therefore, it is necessary to test the feasibility of using data from new sensors for these drought monitoring methods and evaluate the comparability of the drought monitoring results between MODIS and new satellite sensors.

Sentinel-3 is a satellite with high-temporal resolution that was developed by the European Space Agency and recently launched. Sentinel-3 can be used for frequent monitoring of land, ocean, and the atmosphere [14], [15]. Sentinel-3A and Sentinel-3B were launched on February 16, 2016, and April 25, 2018, respectively. The sensors on Sentinel-3 include the ocean and land colour imager (OLCI), the sea and LST radiometer (SLSTR), and the Synthetic aperture radar altimeter. The temporal resolution of a single Sentinel-3 satellite is less than 2.8 days, and the combination of Sentinel-3A and Sentinel-3B can provide a temporal resolution of less than 1.4 days. Compared to MODIS sensors, Sentinel-3 OLCI provides a spatial resolution of approximately 300 m in 21 bands from visible to near-infrared, thus resulting in a higher capability to capture spatial detail. SLSTR provides thermal infrared data with a spatial resolution of 1000 m similar to that of MODIS.

The OLCI Level-2 products from Sentinel-3A have been available since November 29, 2017, and the SLSTR Level-2 LST products from Sentinel-3A have been available since September 8, 2017. The OLCI Level-2 products and SLSTR Level-2 LST products from Sentinel-3B have been available since January 22, 2019 and February 25, 2019, respectively. At the time of writing, there are single-year of Sentinel-3A OLCI Level-2 products and SLSTR Level-2 LST products. Therefore, drought monitoring results cannot be obtained for a multiyear Sentinel-3 VTCI, as can be done for AVHRR and MODIS data. It is necessary to compare the similarity between the Sentinel-3 VTCI and MODIS VTCI and analyze the feasibility of calculating the multiyear Sentinel-3 VTCI for quantitative drought monitoring based on multiyear Terra MODIS data.

The aims of this article are to investigate the methods for calculating the multiyear Sentinel-3 VTCI based on multiyear Terra MODIS data and test the capability of multiyear Sentinel-3 VTCI for drought monitoring using multiyear Terra MODIS VTCI and cumulative precipitation data. Therefore, the objectives are to 1) compare the similarity between the single-year Sentinel-3 VTCI and Terra MODIS VTCI and the similarity of warm edges and cold edges for calculating the single-year VTCIs derived from Sentinel-3 and Terra MODIS in the same period; 2) calculate the multiyear Sentinel-3 VTCI based on multiyear Terra MODIS data and analyze the difference between the single-year Sentinel-3 VTCI and multiyear Sentinel-3 VTCI; and 3) test the capability of multiyear Sentinel-3 VTCI for drought monitoring using the multiyear Terra MODIS VTCI and cumulative precipitation data.

II. Study Area and Data

A. *Study Area*

The study was conducted in the Guanzhong Plain with an average elevation of 500 m, which is located in Shaanxi Province, China (see Fig. 1). The climate is continental monsoon, with cold and dry winters and warm and rainy summers. The average annual rainfall in this plain ranges from 500 to 700 mm, with an average annual temperature of approximately 13 °C. Up to 70% of the land in the Guanzhong Plain is covered by cropland, which includes both irrigated and rainfed cropland. The Guanzhong Plain belongs to a semi-humid area. More than 50% of the croplands in the Guanzhong Plain are rainfed. Most of the croplands in the east are rainfed, while there are many irrigated croplands in the west and middle. The main cropping pattern in this plain is winter wheat in rotation with summer maize. In general, winter wheat is sown from early October to mid-October and harvested in early June of the following year [10], [16].

B. *Remote Sensing Data*

Sentinel-3A images (OLCI and SLSTR) acquired in 2018 and Terra MODIS images acquired over the past 18 years were utilized for drought monitoring. The growth period of winter wheat from the reviving stage to milk stage is from early March to early June; thus, only the images in this period of each year were utilized in this study. The acquisition dates of the Sentinel-3 and MODIS data acquired in the morning at nadir and near-nadir views under clear-sky conditions are shown in Table I, in which there are eleven days overpassed by both Sentinel-3 and MODIS, and the quantity of MODIS data is greater than that of Sentinel-3 data in the study period due to the high temporal resolution. Because there is only one Sentinel-3 image in late April, which cannot represent the drought conditions over a 10-day period, the Sentinel-3 image from late April was not utilized in this study. The Terra MODIS products were downloaded from Atmosphere Archive & Distribution System Distributed Active Archive Center (https://ladsweb.modaps.eosdis.nasa.gov/search/), which include the collection of six reflectance product with 500- and 1000-m

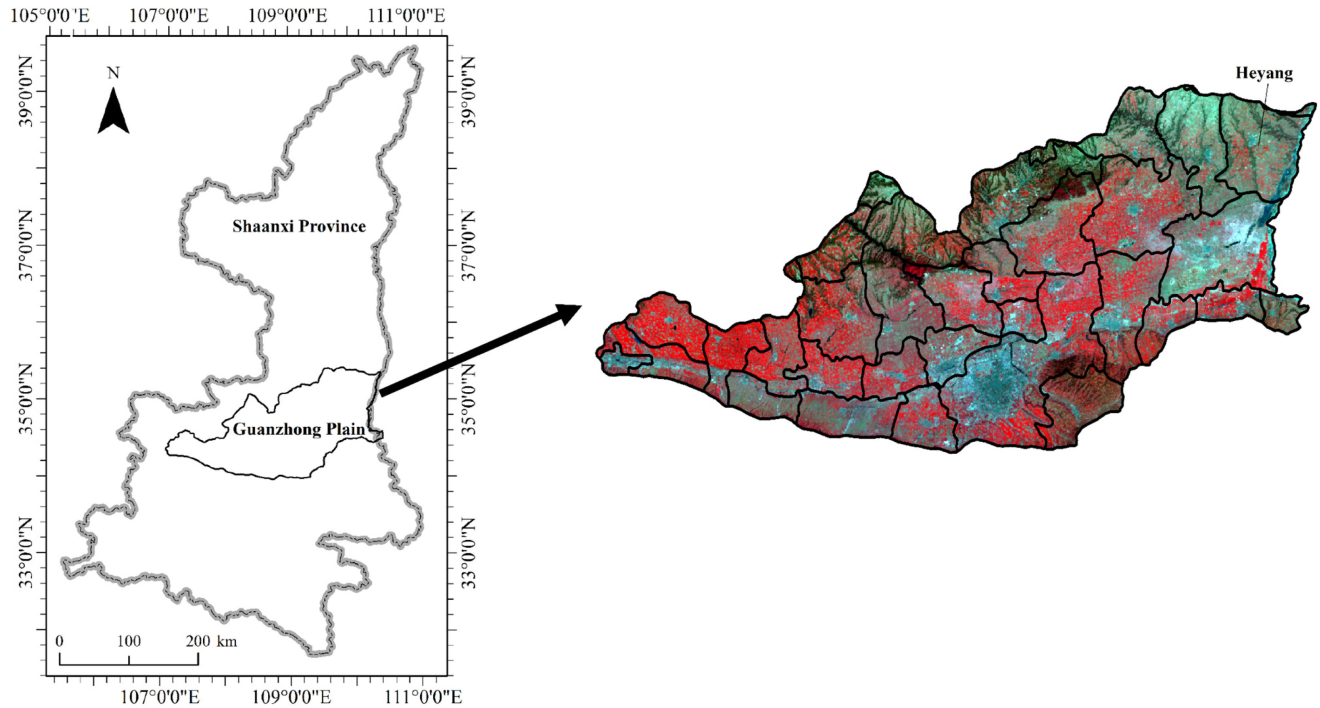

Fig. 1. Location of the Guanzhong Plain in Shaanxi Province, China. The right figure is the false color composite imagery of the Guanzhong Plain on April 9, 2018 using the band 6, 10, and 17 of Sentinel-3 OLCI product.

TABLE I
ACQUISITION DATES OF SENTINEL-3 AND MODIS DATA UNDER CLEAR SKY CONDITIONS

Time period	Sentinel-3	Terra MODIS
Mid-March	13, 14	13, 14, 15
Late March	22, 29	22, 27, 28, 29
Early April	2, 9	2, 3, 4, 8, 9, 10
Mid-April	17, 18	15, 16, 17, 18, 19
Late April	29	21, 26, 27, 29
Early May	2, 3	2, 3

spatial resolution (MOD09GA) and the LST product with 1000-m spatial resolution (MOD11A1). The Sentinel-3 OLCI Level-2 land products with 300-m spatial resolution (OL_2_LFR) and the SLSTR Level-2 LST products with 1000-m spatial resolution were downloaded from the Sentinels Scientific Data Hub (https://scihub.copernicus.eu/). The reflectance of the red and near-infrared bands (RC681 and RC865) in the OLCI Level-2 product are both largely corrected for atmospheric and angular effects. During the preprocessing of these data, both Sentinel-3 products and MODIS products were transformed to the Lambert azimuthal equal-area projection with a spatial resolution of 1000 m, which is conducive to making area comparisons from imagery.

In this article, multiyear Terra MODIS reflectance and LST data were used to calculate multiyear Sentinel-3 VTCI by providing quantitative drought monitoring results over the past several years and test the capability of multiyear Sentinel-3 VTCI for drought monitoring.

C. Precipitation Data

There are 32 meteorological stations in the Guanzhong Plain, which are located in each county of the plain. The daily precipitation data in the study period from March to May 2018 measured by the meteorological stations in 20 counties with rainfed croplands on this plain were used to analyze the capability of multiyear Sentinel-3 VTCI for drought monitoring. In the counties with rainfed croplands, precipitation is the key influence factor of drought. To remain consistent with the temporal scale of VTCI, similar to the methods in the study by Sun *et al.* [10], the precipitation data were processed into 10-day and 20-day cumulative precipitation data.

III. METHODS

The methods used in this study include the calculation of the multiyear Sentinel-3 VTCI and the validation of its capability for drought monitoring. The flowchart of the entire process is shown

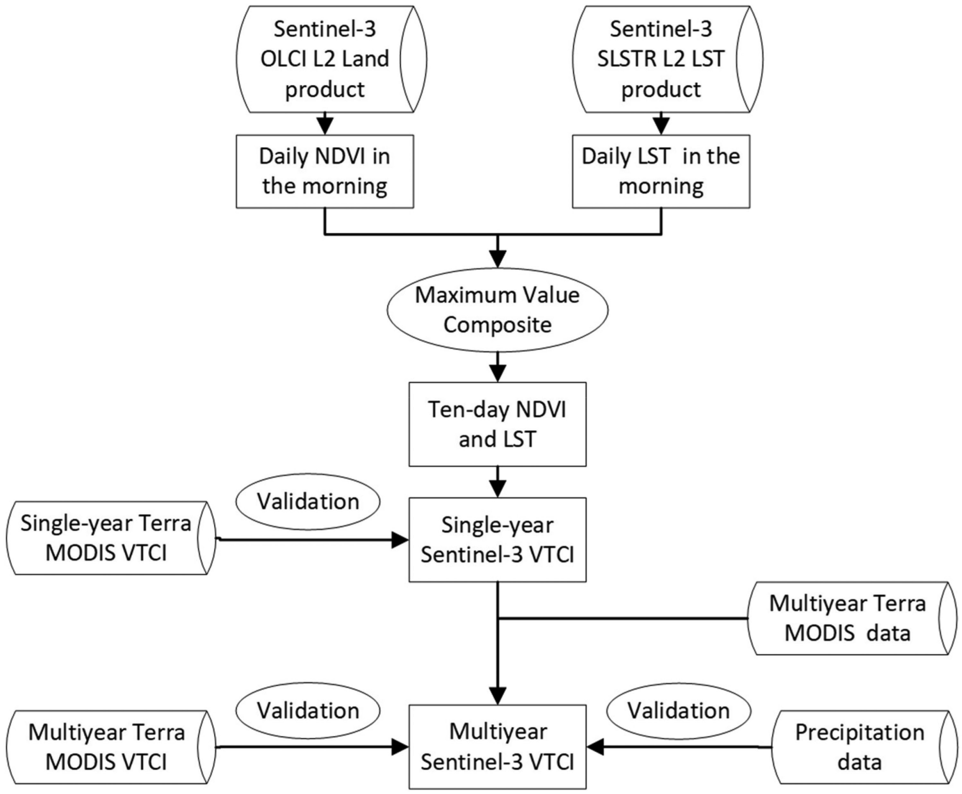

Fig. 2. Multiyear Sentinel-3 VTCI calculation and validation flowchart.

in Fig. 2. First, the daily NDVI and LST data in the morning were obtained from the Sentinel-3 OLCI Level 2 Land product and SLSTR Level 2 LST product, respectively. To reduce the effects from the solar elevation angle, satellite observation angle, orbit drift, clouds, and shadows, the 10-day maximum NDVI and LST products were generated using the maximum value composite (MVC) approach [17], [18]. The single-year Sentinel-3 VTCI was then calculated using the 10-day MVC products. To obtain the multiyear Sentinel-3 VTCI, the multiyear Terra MODIS data were used to calculate the multiyear Sentinel-3 VTCI. Finally, the drought monitoring results from the multiyear Sentinel-3 VTCI were evaluated by comparing them with the multiyear Terra MODIS VTCI and cumulative precipitation data. The key sections of the method are described below.

A. Calculation of VTCI

The VTCI is defined as [9]–[11]

$$\mathrm{VTCI} = \frac{\mathrm{LST}_{\max}(\mathrm{NDVI}_i) - \mathrm{LST}(\mathrm{NDVI}_i)}{\mathrm{LST}_{\max}(\mathrm{NDVI}_i) - \mathrm{LST}_{\min}(\mathrm{NDVI}_i)} \quad (1)$$

where

$$\mathrm{LST}_{\max}(\mathrm{NDVI}_i) = a + b\mathrm{NDVI}_i \quad (2)$$

$$\mathrm{LST}_{\min}(\mathrm{NDVI}_i) = a' + b'\mathrm{NDVI}_i \quad (3)$$

where $\mathrm{LST}_{\max}(\mathrm{NDVI}_i)$ and $\mathrm{LST}_{\min}(\mathrm{NDVI}_i)$ are the maximum and minimum LSTs of the pixels that have the same NDVI_i, respectively. $\mathrm{LST}(\mathrm{NDVI}_i)$ is the LST of one pixel with NDVI value NDVI_i. Coefficients a, b, a', and b' are estimated from the study area where the surface soil moisture spans from wilting point to field capacity. The NDVI is calculated as follows:

$$\mathrm{NDVI} = \frac{\rho(\mathrm{NIR}) - \rho(\mathrm{red})}{\rho(\mathrm{NIR}) + \rho(\mathrm{red})} \quad (4)$$

where $\rho(\mathrm{NIR})$ and $\rho(\mathrm{red})$ are the reflectances of the near-infrared band and red band, respectively. For the MOD09GA products, the first two bands were used to calculate NDVI, and for Sentinel-3 OLCI, RC681, and RC865 were used to calculate NDVI.

One of the key issues in drought monitoring using the VTCI is the determination of warm edges and cold edges. In this study, the warm edges and cold edges for calculating the VTCI are determined according to the methods of Sun *et al.* [10]. The warm edges and cold edges for calculating the Sentinel-3 VTCI can be determined from the data from only 2018 because there are currently only one year of Sentinel-3 OLCI reflectance data and SLSTR LST data. However, the warm edges and cold edges for calculating the Terra MODIS VTCI can be determined from the data over the past 18 years. For a single-year VTCI, the warm edges and cold edges were determined using the MVC NDVI and LST in each 10-day interval of 2018. For the multiyear VTCI, the warm edges were determined using the multiyear MVC NDVI and LST, and the cold edges were determined using the multiyear MVC NDVI and the multiyear maximum–minimum value composite LST [10]. To obtain the multiyear Sentinel-3 VTCI similar to the MODIS VTCI, two methods can be used to combine the single-year Sentinel-3 VTCI with the multiyear Terra MODIS data.

1) If there is a good linear correlation between the single-year VTCI and multiyear VTCI derived from Terra MODIS, then the multiyear Sentinel-3 VTCI can be derived from the single-year Sentinel-3 VTCI according to the linear correlation between the single-year VTCI and multiyear VTCI derived from Terra MODIS, which is called method 1. 2) If the slope and intercept of warm edges and cold edges for calculating the single-year Sentinel-3 VTCI and single-year Terra MODIS VTCI are the same, the warm edges and cold edges for the multiyear Terra MODIS VTCI can be directly used to calculate the multiyear Sentinel VTCI, which is called method 2.

B. Comparison of VTCIs Derived From Sentinel-3 and Terra MODIS

The comparison of the Sentinel-3 VTCI and Terra MODIS VTCI included a comparison of the single-year Sentinel-3 VTCI and single-year Terra MODIS VTCI, a comparison of the single-year VTCI and multiyear VTCI both derived from Terra MODIS and Sentinel-3, and a comparison of the multiyear Sentinel-3 VTCI and multiyear Terra MODIS VTCI. Among these comparisons, the first was used to evaluate the consistency of the single-year VTCIs derived from Sentinel-3 and Terra MODIS and the feasibility of calculating the multiyear Sentinel-3 VTCI using methods 1 and 2. The second comparison was used to analyze the linear correlation between the single-year VTCI and multiyear VTCI derived from Terra MODIS; therefore, the feasibility of calculating the multiyear Sentinel-3 VTCI using methods 1 was analyzed. The second comparison also analyzed the advantages of the multiyear Sentinel-3 VTCI compared to single-year Sentinel-3 VTCI. The third comparison was used to analzse the differences in the drought monitoring results between the multiyear Terra MODIS VTCI and multiyear Sentinel-3 VTCI calculated using methods 1 and 2, thereby testing the capability of multiyear Sentinel-3 VTCI for drought monitoring.

To quantitatively achieve these assessments, the root mean square error (RMSE), average bias, and RMSE of the fit between the Sentinel-3 and Terra MODIS data were used in this study. RMSE is an important indicator for quantifying the difference between estimated and reference values. Average bias is the mean difference between estimated and reference values, which shows the tendency of the model to underestimate or overestimate the reference values. The RMSE of the fit is the RMSE between reference values and the fitted values derived from the estimated values based on the correlation between the estimated values and reference values, which can largely reflect the random error of the estimated values. In the comparison of the NDVIs, LSTs, and VTCIs derived from Sentinel-3 and Terra MODIS, the estimated values represent the Sentinel-3 values, and the reference values represent the Terra MODIS values. In the comparison of the single-year VTCI and multiyear VTCI, the estimated values represent the single-year VTCI, and the reference values represent the multiyear VTCI.

To display the size relationship between Sentinel-3 VTCI and Terra MODIS VTCI and the size relationship between single-year VTCI and multiyear VTCI more intuitively, difference frequency histograms were drawn in this study. If the VTCI difference is concentrated at approximately 0, there is no obvious systematic deviation between the values. However, if the VTCI difference is mostly distributed around [-1, 0] or [0, 1], there are significant systematic deviations between the values.

C. Correlation Analysis Between VTCI and Precipitation

Linear regression was applied to link the multiyear Sentinel-3 VTCI with cumulative precipitation to evaluate the capability of multiyear Sentinel-3 VTCI for quantitative drought monitoring. In this study, the multiyear Sentinel-3 VTCIs with 10-day intervals in the study period from March to May 2018 were linearly regressed with the cumulative precipitation over the previous 10 days and the previous 20 days, respectively. The coefficient of determination (R^2) was used to indicate the correlation between the multiyear VTCI and cumulative precipitation.

In addition, to test the representativeness of the samples used for linear regression analysis, the hypothesis test was used in this study, in which the P-value reflects the probability that the differences between the samples are caused by the sampling errors. Normally, $P < 0.05$ is considered to be significant, and $P < 0.01$ is considered to be very significant.

IV. Results

A. Comparison of NDVIs and LSTs Derived From Sentinel-3 and Terra MODIS

As described in Section II-B, ten days of data acquired in the morning at nadir and near-nadir views under clear-sky conditions in the study period were selected to test the comparability of NDVIs and LSTs derived from Sentinel-3 and Terra MODIS. The RMSEs, average biases, and RMSEs of the fit for NDVI and LST between MODIS and Sentinel-3 for the ten selected days are shown in Table II. The RMSEs of NDVI between MODIS and Sentinel-3 are from 0.080 to 0.109. Furthermore, the average biases between the two sensors are much smaller than the RMSEs, and the RMSEs are very close to the RMSEs of the fit, which indicates that there is no significant systematic deviation in NDVI between the two sensors. The RMSEs of the fit for the ten selected days also changed very little, which indicates that the magnitude of the random differences in NDVI between the two sensors does not substantially change with date and vegetation growth.

For the LST, the absolute values of the average bias are significantly greater than zero and close to the RMSEs on many dates, which indicates that there are significant systematic deviations in LST between the two sensors on these dates. Because the LST is strongly influenced by the duration of sunlight, these systematic differences in the LST can be due to the different overpass times of Sentinel-3 and MODIS. In addition, these systematic differences in LST can also be due to the algorithmic differences and the effect of cloud. The RMSEs of the fit reflect the random deviations in the LST, which indicate that the random differences in LST between Sentinel-3 and MODIS are close to 1 K on most dates. Many studies have validated that the RMSEs of MODIS LST C6 products are less than 1 K in most land

TABLE II
RMSEs, Average Biases, and RMSEs of the Fit in NDVI and LST Between Sentinel-3 and Terra MODIS

Date	NDVI			LST (K)		
	RMSE	Average bias	RMSE of fitting	RMSE	Average bias	RMSE of fitting
Mar. 13th	0.080	0.007	0.063	1.303	-0.797	0.950
Mar. 14th	0.088	0.037	0.070	1.544	-0.315	1.277
Mar. 22nd	0.109	0.064	0.069	1.247	-0.630	1.020
Mar. 29th	0.090	0.037	0.070	1.462	1.096	0.887
Apr.2nd	0.082	0.031	0.059	3.147	2.910	1.110
Apr. 9th	0.082	0.014	0.066	1.986	1.370	1.381
Apr. 17th	0.091	0.015	0.079	1.369	0.870	0.855
Apr. 18th	0.102	0.067	0.070	2.945	2.758	0.892
May.2nd	0.102	0.040	0.076	2.227	0.494	2.122
May 3rd	0.091	0.040	0.073	3.010	2.107	2.073

TABLE III
Warm Edges and Cold Edges for the Sentinel-3 VTCI and Terra MODIS VTCI

Time period	Edges for VTCI	Single-year Sentinel-3	Single-year Terra MODIS	Multiyear Terra MODIS
Mid-March	Warm edge	LST = -13 NDVI + 312	LST = -13 NDVI + 311	LST = -15 NDVI + 316
	Cold edge	LST = 295	LST = 297	LST = 282
Late March	Warm edge	LST = -14 NDVI + 315	LST = -14 NDVI + 314	LST = -17 NDVI + 317
	Cold edge	LST = 296	LST = 297	LST = 288
Early April	Warm edge	LST = -17 NDVI + 320	LST = -17 NDVI + 321	LST = -21 NDVI + 323
	Cold edge	LST = 295	LST = 297	LST = 290
Mid-April	Warm edge	LST = -11 NDVI + 316	LST = -11 NDVI + 317	LST = -19 NDVI + 325
	Cold edge	LST = 296	LST = 298	LST = 285
Early May	Warm edge	LST = -20 NDVI + 323	LST = -20 NDVI + 322	LST = -20 NDVI + 328
	Cold edge	LST = 292	LST = 294	LST = 292

types and could exhibit large errors in bare soil areas [19], [20]. In addition, considering that changes in weather, soil moisture, and other factors may cause differences between MODIS and Sentinel-3 LST, the error of Sentinel-3 LST can be similar to that of MODIS LST.

In summary, the differences in NDVI between Sentinel-3 and Terra MODIS are relatively stable because of the stable RMSE and small average bias. However, the differences in LST between the two sensors are not as stable as the differences in NDVI, which vary with the satellite overpass times. Over a 10-day period, satellite sensors have more opportunities to capture the largest LSTs in the current period. Therefore, during the process of calculating the VTCI, the MVC in each 10-day period could reduce the differences in NDVI and LST between Sentinel-3 and Terra MODIS caused by the differences in overpass time. Therefore, the MVC is important for improving the reliability of the VTCI and the consistency of the VTCI between different sensors.

B. Determination of Warm Edges and Cold Edges for Sentinel-3 and Terra MODIS

The warm edges and cold edges for calculating the Sentinel-3 and Terra MODIS VTCIs were determined as described in Section III-A, including the single-year warm and cold edges and the multiyear warm and cold edges (see Table III). The slopes of the warm edges for the Sentinel-3 VTCI are essentially the same as those for the single-year Terra MODIS VTCI. The intercepts of the warm and cold edges can vary slightly due to the differences in satellite overpass time. As shown in Table II, the average deviation between Sentinel-3 and Terra MODIS LST on the same date can reach 2.910 K. In addition, because the LST largely changes over the years, using multiyear data to determine the warm edges and cold edges can reflect the variations in the LST in the study region over the years, thereby quantitatively reflecting the level of temperature-related drought. As shown in Table III, the absolute values of the slopes and intercepts of the multiyear warm edges for the Terra MODIS VTCI are significantly larger than those of the single-year warm edges, and the intercepts of the multiyear cold edges for the Terra MODIS VTCI are also significantly smaller than those of the single-year cold edges. In early March, the difference in the intercepts between the single-year warm edges and multiyear warm edges is approximately 5 K, and the difference in the intercepts between the single-year cold edges and multiyear cold edges is approximately 14 K, which indicates that the overall LSTs are close to the multiyear warm edges. By the beginning of May, the difference in the intercept between the single-year

TABLE IV
RMSEs, Average Biases, and RMSEs of the Fit Between the Single-Year VTCIs Derived From Sentinel-3 and Terra MODIS

Time period	RMSE	Average bias	RMSE of the fit
Mid-March	0.120	0.007	0.114
Late March	0.150	0.040	0.127
Early April	0.128	0.058	0.109
Mid-April	0.154	0.036	0.133
Early May	0.129	-0.040	0.117

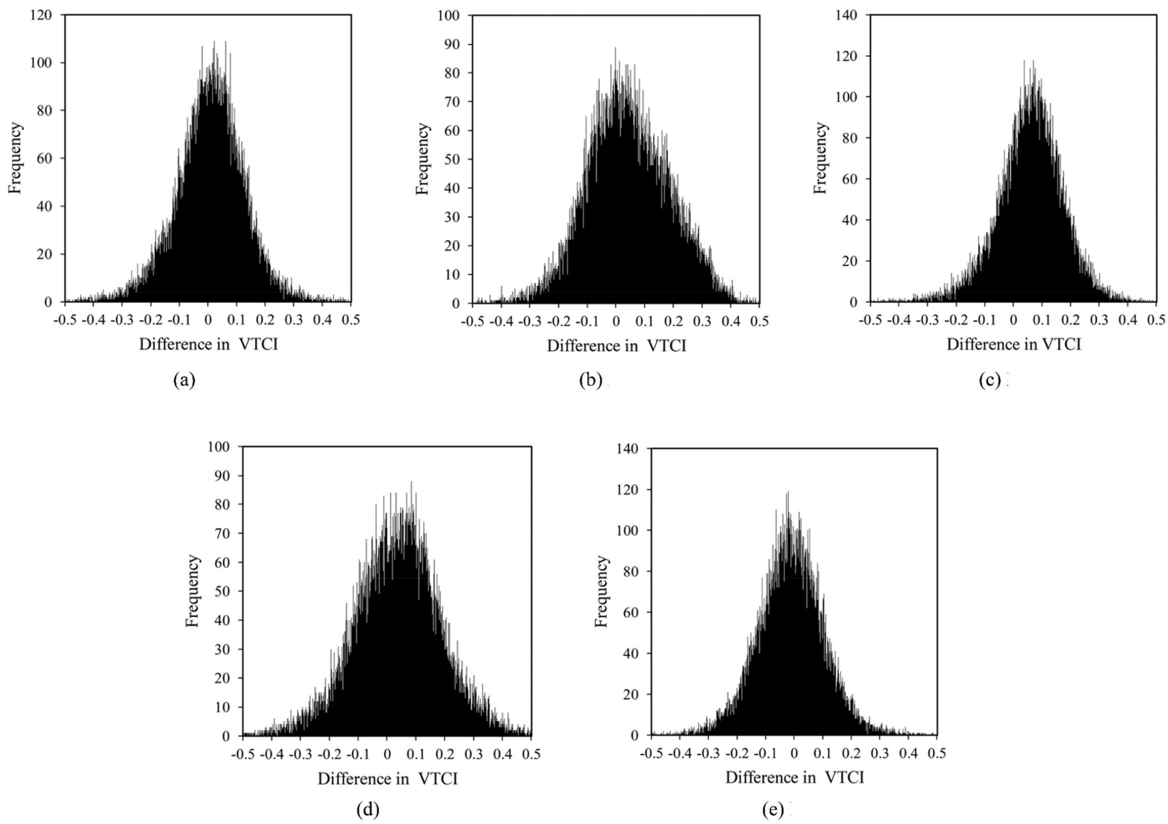

Fig. 3. Difference frequency histograms of the single-year VTCIs derived from Sentinel-3 and Terra MODIS. (a) Mid-March. (b) Late March. (c) Early April. (d) Mid-April. (e) Early May.

warm edge and multiyear warm edge is approximately 6 K, and the difference in the intercept between the single-year cold edge and multiyear cold edge is within 2 K, which indicates that the overall LSTs are close to the multiyear cold edge. All these results indicate that the temperature-related drought decreased from mid-March to early May in the study area.

C. Comparison of Single-Year VTCIs Derived From Sentinel-3 and MODIS

The single-year warm edges and cold edges determined in the previous section were used to calculate the single-year Sentinel-3 VTCI and Terra MODIS VTCI. The RMSEs, average biases, and RMSEs of the fit between the single-year VTCIs derived from Sentinel-3 and Terra MODIS in each 10-day period of the study period are shown in Table IV. In the different 10-day periods of the study period, the RMSEs between the single-year Sentinel-3 VTCI and single-year Terra MODIS VTCI range from 0.120 to 0.154, which indicates that there are large differences between them. In addition, the average biases are much smaller than the RMSEs, and the RMSEs are very close to the RMSEs of the fit, which indicates that the systematic deviations between the single-year Sentinel-3 VTCI and the single-year Terra MODIS VTCI are very small. Moreover, the RMSEs between the single-year Sentinel-3 VTCI and single-year Terra MODIS VTCI are mainly due to random deviations.

The frequency histograms of the differences between the single-year Sentinel-3 VTCI and single-year Terra MODIS VTCI are shown in Fig. 3. Except for early April, the VTCI differences with the greatest frequencies are close to 0, which indicates that there are no significant systematic deviations between the single-year VTCI and single-year Terra MODIS VTCI in most 10-day periods. In addition, because the warm edges and cold edges for calculating the single-year Sentinel-3

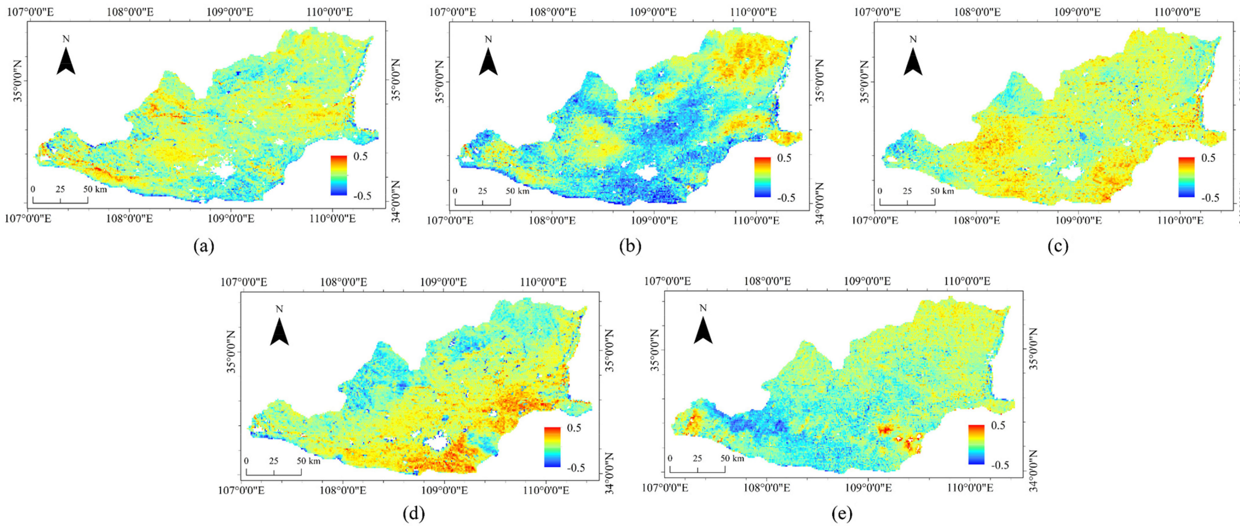

Fig. 4. Spatial distributions of the differences between the single-year VTCIs derived from Sentinel-3 and Terra MODIS. (a) Mid-March. (b) Late March. (c) Early April. (d) Mid-April. (e) Early May.

VTCI and Terra MODIS VTCI shown in Table III are basically the same in most 10-day periods, it is feasible to use method 2 to calculate the multiyear Sentinel-3 VTCI.

The spatial distributions of the differences between the single-year Sentinel-3 VTCI and single-year Terra MODIS VTCI are shown in Fig. 4. The distributions of the differences are not uniform, but there are obvious high and low values in some regions, which indicates that the differences between the single-year Sentinel-3 VTCI and Terra MODIS VTCI are not random noise-like differences. Rather, these differences have obvious regional distribution characteristics. For most 10-day periods, the differences in the west and middle are lower than that of the other part, which indicates that these differences between the single-year Sentinel-3 VTCI and Terra MODIS VTCI can be due to the algorithmic differences of LST and the difference of spectral response. In addition, the distributions are different in different 10-day periods, which can be due to the difference of satellite overpass times and the effect of cloud. Combined with the RMSEs and the RMSEs of the fit shown in Table IV, the random deviations between the single-year Sentinel-3 VTCI and single-year Terra MODIS VTCI are large, although the systematic differences between them are very small. These results indicate that the uncertainties of the single-year Sentinel-3 VTCI and single-year Terra MODIS VTCI are large. These uncertainties can be reduced by using the MVC of the LST data; thus, the reliabilities of the VTCI are determined by the quantity of LST data in each 10-day period. Moreover, the Terra MODIS VTCI computed using a large quantity of LST data should be more reliable than the Sentinel-3 VTCI.

D. Relationship Between the Single-Year VTCI and Multiyear VTCI

The two methods described in Section III-A were used to calculate the multiyear Sentinel-3 VTCI. In method 1, a good linear correlation between single-year VTCI and multiyear VTCI derived from Terra MODIS is required. The RMSEs of the fit between the single-year VTCI and multiyear VTCIs derived from Terra MODIS in each 10-day period of the study period are shown in Fig. 5. The RMSEs of the fit between the single-year VTCIs and multiyear VTCIs of Terra MODIS range from 0.010 to 0.030, which indicates that the single-year Terra MODIS VTCIs exhibit good linear correlations with the multiyear Terra MODIS VTCIs. Therefore, it is feasible to use method 1 to calculate the multiyear Sentinel-3 VTCI.

The RMSEs, average biases, and RMSEs of the fit between the single-year Sentinel-3 VTCI and multiyear Sentinel-3 VTCIs calculated using methods 1 and 2 in each 10-day period of the study period are shown in Table V. Because the multiyear Sentinel-3 VTCI calculated using method 1 was directly derived from the linear transformation of the single-year Sentinel-3 VTCI, the RMSE of the fit between them is 0. For method 2, which uses the warm edges and cold edges of the multiyear Terra MODIS VTCI to calculate the multiyear Sentinel-3 VTCI, the RMSEs of the fit between the single-year VTCIs and multiyear VTCIs derived from Sentinel-3 range from 0.014 to 0.037. These results indicate that the single-year Sentinel-3 VTCIs exhibit a good linear correlation with the multiyear Sentinel-3 VTCIs calculated using method 1 or method 2. In addition, the RMSEs between the single-year VTCI and multiyear VTCI in different 10-day periods are significantly larger than the RMSEs of the fit, and the absolute values of the average biases are significantly greater than 0. These results indicate that there are significant systematic deviations between the single-year Sentinel-3 VTCI and multiyear Sentinel-3 VTCI. The single-year Sentinel-3 VTCI reflects the relatively dry–wet distribution, while the multiyear Sentinel-3 reflects the levels of temperature-related drought over multiple years. The variation in the systematic deviations between the single-year Sentinel-3 VTCI and multiyear Sentinel-3 VTCI at different 10-day periods reflect the variation in the temperature-related drought levels.

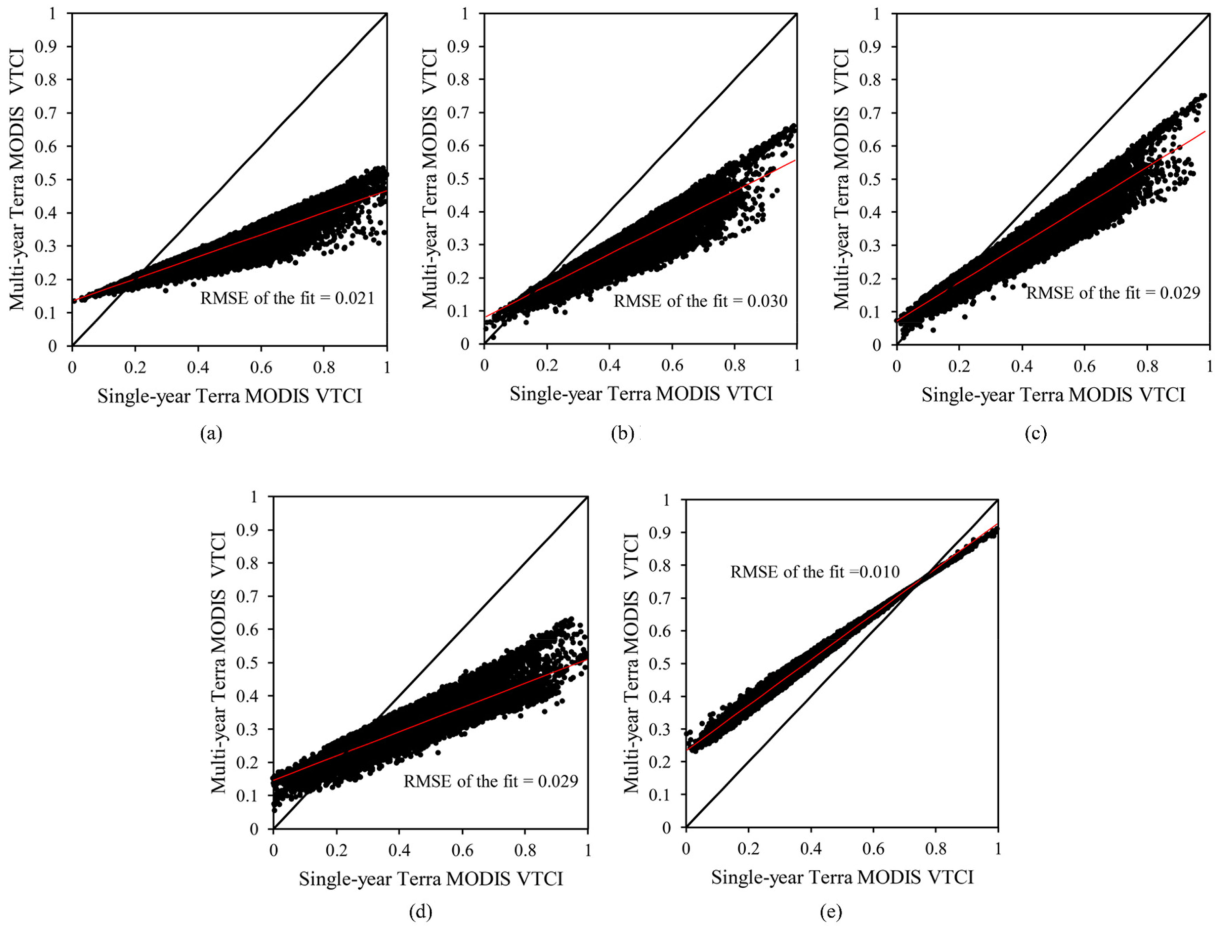

Fig. 5. RMSEs of the fit between the single-year VTCI and multiyear VTCI derived from Terra MODIS. (a) Mid-March. (b) Late March. (c) Early April. (d) Mid-April. (e) Early May.

TABLE V
RMSES, AVERAGE BIASES, AND RMSES OF THE FIT BETWEEN THE SINGLE-YEAR SENTINEL-3 VTCI AND MULTIYEAR SENTINEL-3 VTCI

Time period	Method 1 (based on the linear correlation between the single-year and multiyear VTCI)			Method 2 (using the edges of Terra MODIS directly)		
	RMSE	Average bias	RMSE of the fit	RMSE	Average bias	RMSE of the fit
Mid-March	0.229	0.210	0.000	0.210	0.194	0.023
Late March	0.187	0.173	0.000	0.191	0.179	0.037
Early April	0.133	0.118	0.000	0.094	0.074	0.027
Mid-April	0.176	0.145	0.000	0.140	0.098	0.027
Early May	0.125	-0.117	0.000	0.133	-0.130	0.014

E. Comparison of Multiyear VTCIs Derived From Sentinel-3 and Terra MODIS

The RMSEs, average biases, and RMSEs of the fit between the multiyear Terra MODIS VTCI and multiyear Sentinel-3 VTCIs calculated by methods 1 and 2 in each 10-day period of the study period are shown in Table VI. The RMSEs of the fit between the multiyear Terra MODIS VTCI and multiyear Sentinel-3 VTCI calculated using method 1 range from 0.043 to 0.083, and those between the multiyear Terra MODIS VTCI and multiyear Sentinel-3 VTCI calculated using method 2 range from 0.041 to 0.078. The RMSEs of the fit for these two methods are basically the same, i.e., the random deviations between the multiyear Terra MODIS VTCI and multiyear Sentinel-3 VTCI calculated using method 1 are basically same as those between the multiyear Terra MODIS VTCI and multiyear Sentinel-3 VTCI calculated using method 2. In addition, for method 1, the RMSEs between the multiyear Sentinel-3 VTCI and multiyear Terra MODIS VTCI are basically same as the RMSEs of the fit between them, and the absolute values of the average biases are also very small (no more than 0.035), which indicates that there are very small systematic deviations between the multiyear Terra MODIS VTCI and multiyear Sentinel-3 VTCI calculated using

TABLE VI
RMSES, AVERAGE BIASES, AND RMSES OF THE FIT BETWEEN THE MULTIYEAR TERRA MODIS VTCI AND MULTIYEAR SENTINEL-3 VTCI CALCULATED USING METHODS 1 AND 2

Time period	Method 1 (based on the linear correlation between the single-year and multiyear VTCI)			Method 2 (using the edges of Terra MODIS directly)		
	RMSE	Average bias	RMSE of the fit	RMSE	Average bias	RMSE of the fit
Mid-March	0.044	0.002	0.043	0.053	0.019	0.041
Late March	0.076	0.020	0.066	0.089	0.014	0.067
Early April	0.086	0.035	0.074	0.115	0.078	0.074
Mid-April	0.071	0.014	0.062	0.094	0.060	0.061
Early May	0.092	-0.025	0.083	0.090	-0.013	0.078

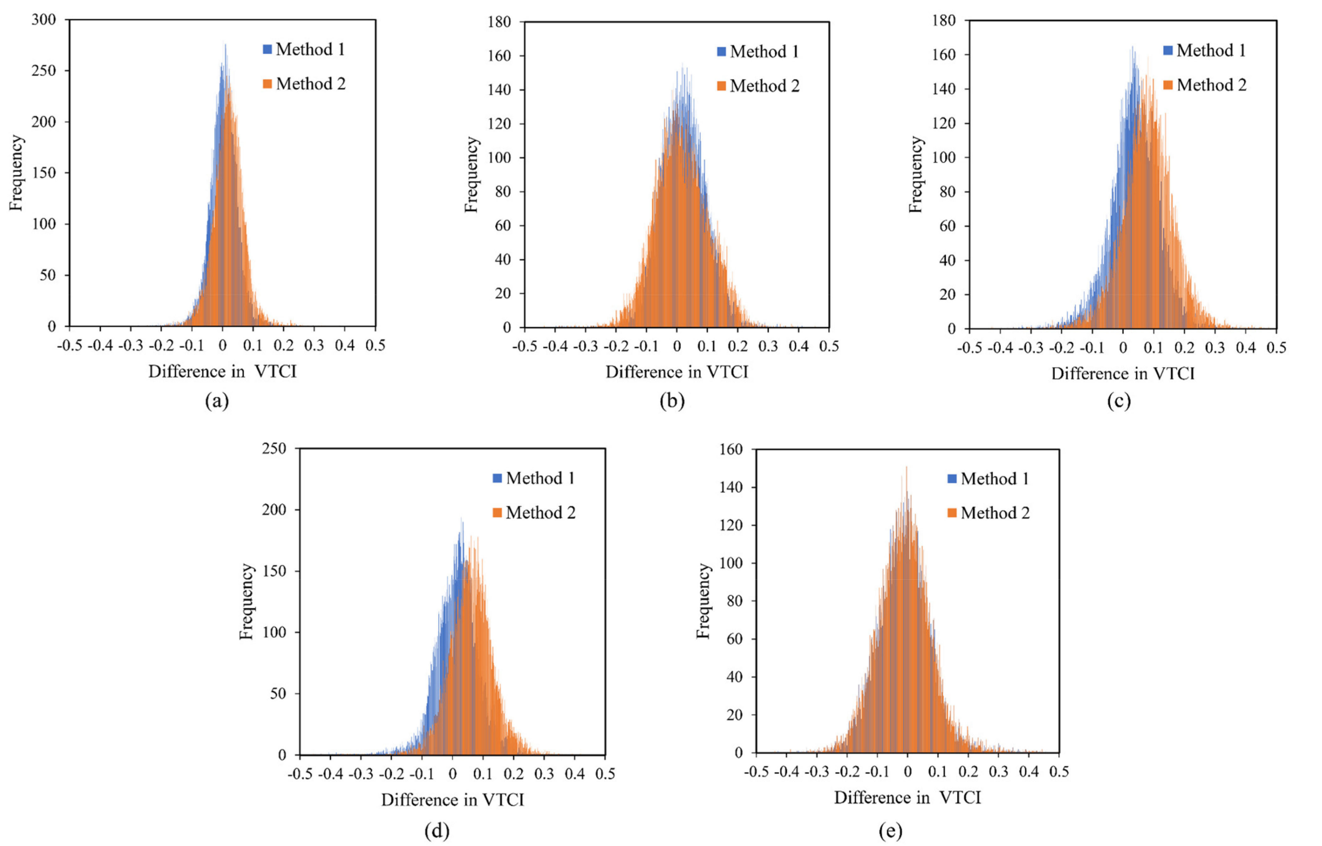

Fig. 6. Difference frequency histograms of the multiyear Terra MODIS VTCI and multiyear Sentinel-3 VTCI calculated using methods 1 and 2. (a) Mid-March. (b) Late March. (c) Early April. (d) Mid-April. (e) Early May.

method 1. Therefore, the multiyear Sentinel-3 VTCIs calculated using method 1 closely reflect the drought levels at the Terra MODIS overpass time. For method 2, the RMSEs between the multiyear Sentinel-3 VTCI and multiyear Terra MODIS VTCI are basically same as the RMSEs of the fit VTCI and multiyear Sentinel-3 VTCI calculated using between them in most of the 10-day periods, while the RMSEs are slightly larger than the RMSEs of the fit between them in April. Moreover, the absolute values of the average biases are also obviously larger than 0 in April. These results indicate that there are not obvious systematic deviations between the multiyear Terra MODIS VTCI and multiyear Sentinel-3 VTCI calculated using method 2 in most 10-day periods, but there might be some systematic deviations between them in some 10-day periods due to the differences in the LST at the different satellite overpass times. In method 2, the warm edges and cold edges of the multiyear Terra MODIS VTCI were directly used to calculate the multiyear Sentinel-3 VTCI, which closely reflect the drought levels at the Sentinel-3 overpass time. Thus, there might be some systematic deviations between the multiyear Terra MODIS VTCI and multiyear Sentinel-3 VTCI calculated using method 2.

The frequency histograms of the difference between the multiyear Terra MODIS VTCI and multiyear Sentinel-3 VTCI calculated using methods 1 and 2 are shown in Fig. 6. The peak frequencies of the differences between the multiyear Terra MODIS VTCI and multiyear Sentinel-3 VTCI calculated using method 1 occur close to 0. While for method 2, the peak frequencies of the differences between the multiyear Terra MODIS VTCI and multiyear Sentinel-3 VTCI are not close to 0 in some 10-day periods, which indicates that there are some systematic deviations between the multiyear Terra MODIS VTCI and multiyear Sentinel-3 VTCI calculated using method 2 in these periods. In early and mid-April, more values in the difference frequency histograms are distributed around [0,1], which indicates that the multiyear Sentinel-3 VTCIs are slightly larger than the multiyear Terra MODIS VTCIs. These results are similar to those indicated in Table VI, which indicates that the multiyear Sentinel-3 VTCIs calculated using method 1 are more similar to the multiyear Terra MODIS VTCIs than the multiyear Sentinel-3 VTCIs calculated using method 2 in the study period. Since the MVC of the LST in each 10-day period can increase the reliability of the multiyear VTCI, and there are more Terra MODIS data than Sentinel-3 data in each 10-day period, it can be considered that the drought levels indicated by the multiyear Terra MODIS VTCI are more reliable. Therefore, it is better to calculate the multiyear Sentinel-3 data using method 1. The multiyear Terra MODIS VTCIs and multiyear Sentinel-3 VTCIs calculated using method 1 in each 10-day period of the study period are shown in Fig. 7. The values of the multiyear Sentinel-3 VTCI calculated using method 1 are similar to the values of the multiyear Terra MODIS VTCI in most 10-day periods, which indicates that there is good consistency between the multiyear Terra MODIS VTCI and the multiyear Sentinel-3 VTCI calculated using method 1. Thus, the multiyear Sentinel-3 VTCI and multiyear Terra MODIS VTCI approximately reflect the drought levels in the same moment. The drought in the west and middle of the Guanzhong Plain is lighter than that in the east since early April, which is consistent with farming management practices. Most of the croplands in the west and middle are irrigated, while most of the croplands in the east are rainfed [10]. In the study period, the droughts in the Guanzhong Plain are more severe before mid-April, after which the occurrence of drought is reduced. By early May, the droughts in this plain are much lighter than those in March and April. These results are correlated with the cumulative precipitation in the study periods, which are analysed in the next section.

F. Precipitation and Multiyear Sentinel-3 VTCI

The linear correlation between the cumulative precipitation over the past 20 days and the multiyear Sentinel-3 VTCIs over 10-day intervals calculated using method 1 in the study period are shown in Fig. 8. The multiyear Sentinel-3 VTCIs over 10-day intervals exhibit a significant correlation with the cumulative precipitation over the past 20 days (R^2 is 0.731, P-value is less than 0.001), in which the data before mid-April are mainly distributed in the lower left part of the figures and the data in early May are mainly distributed in the upper right part of the figures. Similar results can be found in the studies by Lin *et al.* [21] and Khan *et al.* [12]. Heyang is one of the counties with rainfed croplands in the Guanzhong Plain, and it is located in the northeast of the plain as shown in Fig. 1. In most 10-day periods of the study period, the multiyear Sentinel-3 VTCI time series profile in Heyang County has similar fluctuations in the profile of the past 20-day cumulative precipitation (see Fig. 9), which is similar to the results in the study by Sun *et al.* [10]. These results indicate that the multiyear Sentinel-3 VTCI calculated using method 1 is near real-time and can provide quantitative drought monitoring results, and the method for retrieving the multiyear Sentinel-3 VTCIs is applicable for quantitative drought monitoring in the study region.

V. Discussion

The multiyear VTCIs derived from AVHRR and MODIS have been successfully applied to drought monitoring and soil moisture retrieval in previous studies. The purpose of this study was to investigate the methods for calculating the multiyear Sentinel-3 VTCI and the capability of multiyear Sentinel-3 VTCI for quantitative drought monitoring. Two methods are used to calculate the multiyear Sentinel-3 VTCI based on the multiyear Terra MODIS VTCI. Method 1 exhibits greater applicability, while sufficient quantities of Sentinel-3 data are required in each 10-day period for method 2, and the warm edges and cold edges for the single-year Sentinel-3 VTCI are basically the same as those for the single-year Terra MODIS VTCI. However, the quantity of Sentinel-3 data in each 10-day period cannot always satisfy the conditions of method 2 currently. The correlation analysis between the multiyear Sentinel-3 VTCI and cumulative precipitation indicates that the multiyear Sentinel-3 VTCI has good capability to quantitatively monitor the drought levels in the study period. Therefore, Sentinel-3 data can be another high-quality remote sensing data source for VTCI drought monitoring in addition to MODIS data. When there are not enough multiyear Sentinel-3 data, Terra MODIS data can be used to assist with the calculation of the multiyear Sentinel-3 VTCI. The reliability of drought monitoring using VTCI is determined by the quantity and quality of the images in each 10-day period because the MVCs of NDVI and LST in each 10-day period are needed to calculate the VTCI. The combination of Sentinel-3 data with Terra MODIS data can provide more images for calculating the VTCI in each 10-day period, thereby further improving the reliability of VTCI drought monitoring.

At present, the Sentinel-3A satellite cannot pass over the study area every day. The quantities of Sentinel-3A data are not sufficient for drought monitoring using VTCI in some periods. With the recent launch of the Sentinel-3B satellite, the amount of Sentinel-3 data will further increase, which can largely improve the reliability of drought monitoring using Sentinel-3 VTCI after the NDVI and LST data from Sentinel-3A and Sentinel-3B are intercalibrated.

Because the spatial resolution of Sentinel-3 and MODIS cannot distinguish croplands from built-up areas and the existence of built-up areas can affect the accuracy of drought monitoring, remote sensing data with both high spatial resolution and high temporal resolution are required for drought monitoring. Spatiotemporal data fusion can be used to fuse satellite data with high spatial resolution but low temporal resolution and data with high temporal resolution but low spatial resolution [22]. There have been many visible and near-infrared remote sensing satellites with high spatial resolution, such as Landsat-8 and

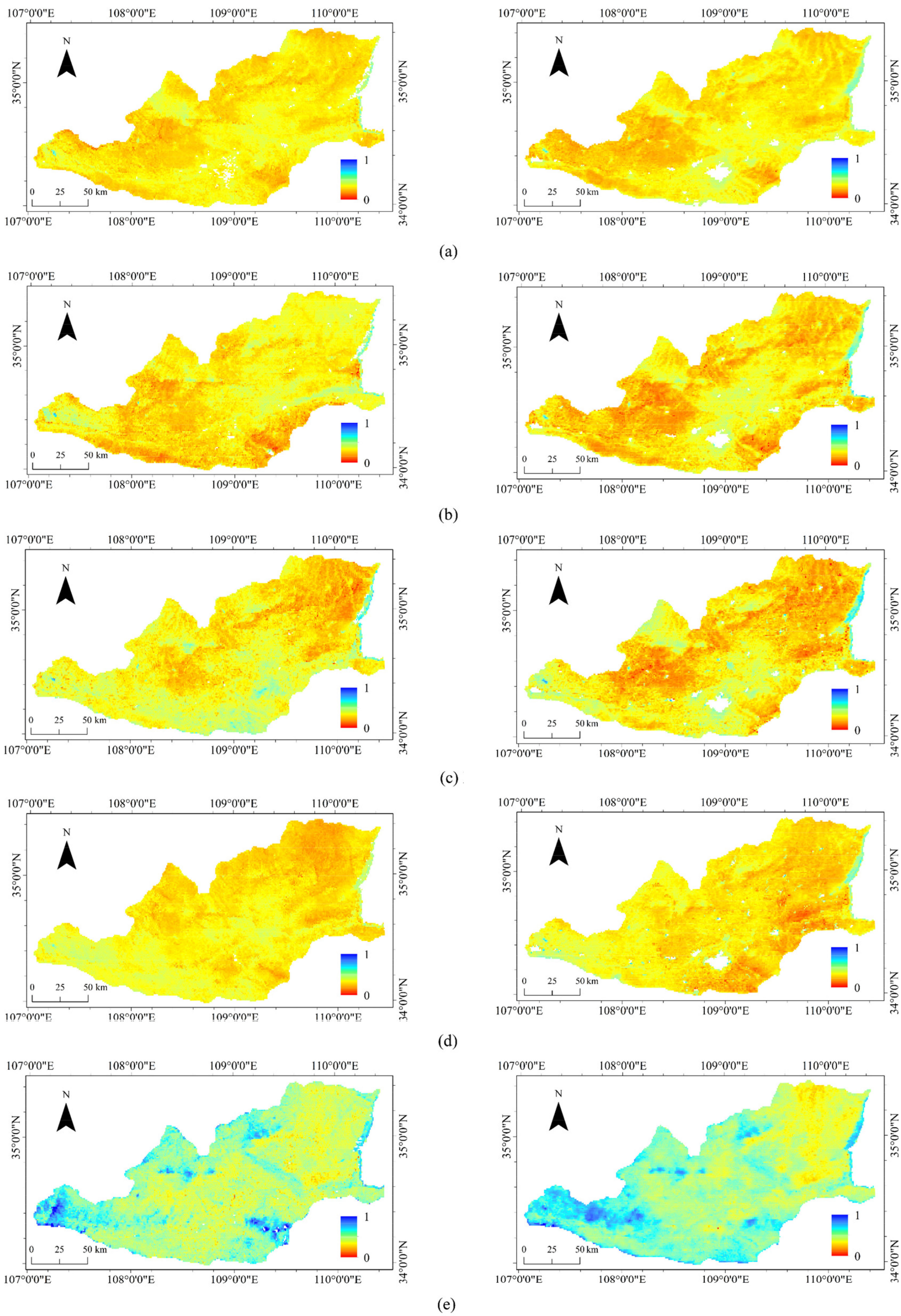

Fig. 7. Multiyear Terra MODIS VTCI and multiyear Sentinel-3 VTCI calculated using method 1. (a) Mid-March. (b) Late March. (c) Early April. (d) Mid-April. (e) Early May.

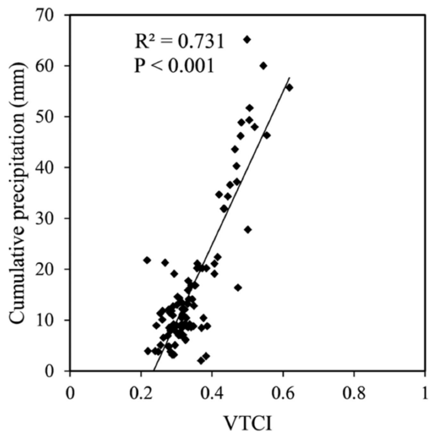

Fig. 8. Correlation between cumulative precipitation over the past 20 days and the multiyear Sentinel-3 VTCI over a 10-day interval calculated using method 1 in the study period.

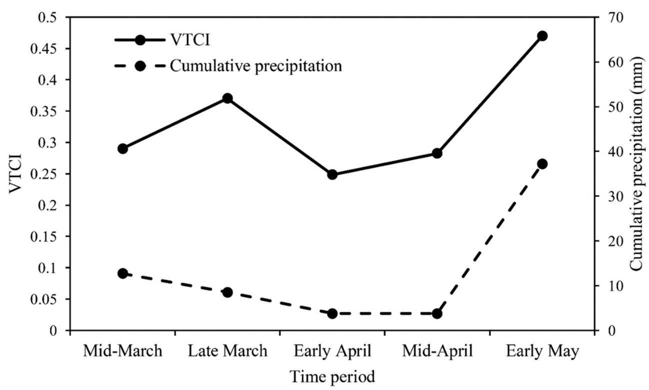

Fig. 9. Time series of cumulative precipitation over the past 20 days and the multiyear Sentinel-3 VTCI over a 10-day interval calculated using method 1 in the Heyang County.

Sentinel-2. For thermal infrared sensors, the spatial resolution of TIRS in Landsat-8 is 100 m, which is the highest spatial resolution of the current thermal infrared sensors. In addition, with the launch of China's Gaofen-5 satellite [23], which has a spatial resolution of 40 m, more thermal infrared sensors with high spatial resolution can be used to improve the spatial resolution of MODIS and Sentinel-3 LST data.

VI. Conclusion

Sentinel-3 is a satellite with thermal infrared sensors onboard with high temporal resolution, which was launched in recent years. In this study, we investigated the methods used to calculate the multiyear Sentinel-3 VTCI and tested the capability of multiyear Sentinel-3 VTCI for drought monitoring by comparing with Terra MODIS VTCI and linking with cumulative precipitation. It is more feasible to calculate the multiyear Sentinel-3 VTCI from the single-year Sentinel-3 VTCI based on the linear correlation between the single-year VTCI and multiyear VTCI derived from Terra MODIS, which do not exhibit obvious systematic deviations from the multiyear Terra MODIS VTCI. The multiyear Sentinel-3 VTCI calculated using the method developed in this article can quantitatively reflect the drought levels near real-time, which exhibit a significant linear correlation with the recent cumulative precipitation in a study period. Our study indicates that Sentinel-3 can successfully inherit the VTCI-based drought monitoring tasks from MODIS once the data are not available. At present, the reliability of drought monitoring using the VTCI can be further improved by combining Terra MODIS VTCI and Sentinel-3 VTCI. In addition, after the launch of the Sentinel-3B satellite, the temporal resolution of Sentinel-3 will be closer to that of MODIS and the reliability of drought monitoring using the VTCI can be further improved. However, similar to MODIS VTCI, the drought monitoring results of the Sentinel-3 VTCI are also strongly affected by the mixed pixels of vegetation and built-up areas. Therefore, it is necessary to use a spatiotemporal data fusion approach to fuse high temporal resolution data with high spatial resolution data in future studies.

References

[1] X. Liu, Y. Pan, X. Zhu, T. Yang, J. Bai, and Z. Sun, "Drought evolution and its impact on the crop yield in the North China plain," *J. Hydrol.*, vol. 564, pp. 984–996, Jul. 2018.

[2] G. Leng and J. Hall, "Crop yield sensitivity of global major agricultural countries to droughts and the projected changes in the future," *Sci. Total Environ.*, vol. 654, pp. 811–821, Mar. 2019.

[3] S. Park, J. Im, E. Jang, and J. Rhee, "Drought assessment and monitoring through blending of multi-sensor indices using machine learning approaches for different climate regions," *Agricultural Forest Meteorol.*, vol. 216, pp. 157–169, Jan. 2016.

[4] S. Park, J. Im, S. Park, and J. Rhee, "Drought monitoring using high resolution soil moisture through multi-sensor satellite data fusion over the Korean Peninsula," *Agricultural Forest Meteorol.*, vol. 237–238, pp. 257–269, May 2017.

[5] F. N. Kogan, "Remote sensing of weather impacts on vegetation in non-homogeneous areas," *Int. J. Remote Sens.*, vol. 11, no. 8, pp. 1405–1419, Aug. 1990.

[6] F. N. Kogan, "Application of vegetation index and brightness temperature for drought detection," *Adv. Space Res.*, vol. 15, no. 11, pp. 91–100, Dec. 1995.

[7] R. R. Gillies and T. N. Carlson, "Thermal remote sensing of surface soil water content with partial vegetation cover for incorporation into climate models," *J. Appl. Meteorol.*, vol. 34, no. 4, pp. 745–756, Apr. 1995.

[8] R. R. Gillies, W. P. Kustas, and K. S. Humes, "A verification of the 'triangle' method for obtaining surface soil water content and energy fluxes from remote measurements of the normalized difference vegetation index (NDVI) and surface surface radiant temperature," *Int. J. Remote Sens.*, vol. 18, no. 15, pp. 3145–3166, Jan. 1997.

[9] P. Wang, J. Gong, and X. Li, "Vegetation-temperature condition index and its application for drought monitoring," *Geomatics Inf. Sci. Wuhan Univ.*, vol. 26, no. 5, pp. 142–148, Oct. 2001.

[10] W. Sun *et al.*, "Using the vegetation temperature condition index for time series drought occurrence monitoring in the Guanzhong plain, PR China," *Int. J. Remote Sens.*, vol. 29, no. 17–18, pp. 5133–5144, Sep. 2008.

[11] Z. Wan, P. Wang, and X. Li, "Using MODIS land surface temperature and normalized difference vegetation index products for monitoring drought in the southern great plains, USA," *Int. J. Remote Sens.*, vol. 25, no. 1, pp. 61–72, Jan. 2004.

[12] J. Khan, P. Wang, Y. Xie, L. Wang, and L. Li, "Mapping MODIS LST NDVI imagery for drought monitoring in Punjab Pakistan," *IEEE Access*, vol. 6, pp. 19898–19911, Apr. 2018.

[13] Y. Xie, P. Wang, H. Sun, S. Zhang, and L. Li, "Assimilation of leaf area index and surface soil moisture with the CERES-wheat model for winter wheat yield estimation using a particle filter algorithm," *IEEE J. Sel. Topics Appl. Earth Observ. Remote Sens.*, vol. 10, no. 4, pp. 1303–1316, Apr. 2017.

[14] M. Berger and J. Aschbacher, "Preface: The Sentinel missions—New opportunities for science," *Remote Sens. Environ.*, vol. 120, pp. 1–2, May 2012.

[15] W. Verhoef and H. Bach, "Simulation of Sentinel-3 images by four-stream surface–atmosphere radiative transfer modeling in the optical and thermal domains," *Remote Sens. Environ.*, vol. 120, pp. 197–207, May 2012.

[16] Y. Xie *et al.*, "Assimilation of the leaf area index and vegetation temperature condition index for winter wheat yield estimation using Landsat imagery and the CERES-Wheat model," *Agricultural Forest Meteorol*, vol. 246, pp. 194–206, Nov. 2017.

[17] B. N. Holben, "Characteristics of maximum-value composite images from temporal AVHRR data," *Int. J. Remote Sens.*, vol. 7, no. 11, pp. 1417–1434, Dec. 1986.

[18] J. Cihlar, D. Manak, and M. D. Iorio, "Evaluation of compositing algorithms for AVHRR data over land," *IEEE Trans. Geosci. Remote Sens.*, vol. 32, no. 2, pp. 427–437, Mar. 1994.

[19] S. Duan, Z. Li, J. Cheng, and P. Leng, "Cross-satellite comparison of operational land surface temperature products derived from MODIS and ASTER data over bare soil surfaces," *ISPRS J. Photogram. Remote Sens.*, vol. 126, pp. 1–10, Feb. 2017.

[20] S. Duan, Z. Li, H. Wu, P. Leng, M. Gao, and C. Wang, "Radiance-based validation of land surface temperature products derived from collection 6 MODIS thermal infrared data," *Int. J. Appl. Earth Observ. Geoinf.*, vol. 70, pp. 84–92, Aug. 2018.

[21] Q. Lin, P. Wang, S. Zhang, L. Li, Y. Jing, and J. Liu, "Applicability of vegetation temperature index for drought monitoring at different time scales," *Arid Zone Res.*, vol. 33, no. 1, pp. 186–192, Jan. 2016.

[22] X. Zhu, F. Cai, J. Tian, and K. A. Williams, "Spatiotemporal fusion of multisource remote sensing data: Literature survey, taxonomy, principles, applications, and future directions," *Remote Sens*., vol. 10, no. 4, Apr. 2018, Art. no. 527.

[23] Y. Chen, S. Duan, H. Ren, J. Labed, and Z. Li, "Algorithm development for land surface temperature retrieval: Application to Chinese Gaofen-5 data," *Remote Sens.*, vol. 9, no. 2, Feb. 2017, Art. no. 161.

Xijia Zhou received the B.S. degree in geographic information system from Capital Normal University, Beijing, China, in 2014, and the M.S. degree in cartography and geographic information system from the Beijing Normal University, Beijing, in 2017. He is currently working toward the Ph.D. degree with China Agricultural University, Beijing, China.

His research interest focuses on quantitative remote sensing.

Pengxin Wang received the B.Sc. and M.Sc. degrees in agronomy from Northwestern Agricultural University, Xianyang, China, in 1988 and 1991, respectively, and the Ph.D. degree in photogrammetry and remote sensing from Wuhan University, Wuhan, China, in 2001.

He has been a Professor with China Agricultural University, Beijing, China, since 2001. From 1991 to 1998, he was a Faculty Member with NWAU. He teaches remote sensing at the undergraduate and graduate levels. His main research interests include the application of quantitative remote sensing in agriculture.

Kevin Tansey received the B.S. degree from the University of Sheffield, Sheffield, U.K., in 1995, and the Ph.D. degree in remote sensing and physical geography from the University of Leicester, Leicester, U.K., in 1999.

He has held research positions at Swansea University (UK), Friedrich-Schiller University (Germany) and the Joint Research Centre of the European Commission, Italy. He is currently Professor of remote sensing with the School of Geography, Geology and the Environment, the University of Leicester. His research interests include remote sensing of land surface dynamics in relation to vegetation growth and disturbance.

Darren Ghent received the B.Sc. degree in mathematics from Loughborough University, Loughborough, Leicestershire, in 1995, the M.Sc. degree in environmental management and Ph.D. degree in physical geography from the University of Leicester, Leicester, U.K., in 2004 and 2010.

He is currently a Senior Research Fellow with the University of Leicester and Staff Member with the National Centre for Earth Observation (NCEO) in the U.K. His research interests include the retrieval, validation, and exploitation of thermal Earth Observation data.

Shuyu Zhang received the B.Sc. degree in electronic engineering and computer science from Northwestern Polytechnical University, Xi'an, China, in 1990.

He is a Researcher with the Remote Sensing Information Center for Agriculture of Shaanxi Province, Xi'an, China. His main research interests include the applications of remote sensing in agriculture and meteorology.

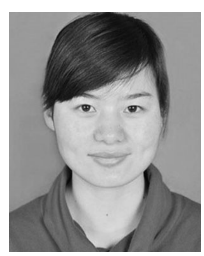

Hongmei Li received the B.S. degree in geographic information system from Northwestern University, Xi'an, China, in 2006, and the M.S. degree in applied meteorology from the Nanjing University of Information Science and Technology, Nanjing, China, in 2015.

She is a Senior Engineer with the Remote Sensing Information Center for Agriculture of Shaanxi Province, Xi'an, China. She is mainly engaged in meteorological services for agricultural remote sensing applications.

Lei Wang received the B.S. degree from the School of Resource Environment and Earth Science, Yunnan University, Kunming, China, in 2012, and the M.S. degree in 2015 from the College of Information and Electrical Engineering, China Agricultural University, Beijing, China, where she is currently working toward the Ph.D. degree.

She is currently a Visiting Student with the Department of Geographical Sciences, University of Maryland at College Park, College Park, MD, USA. Her research interest focuses on quantitative remote sensing.